This is a preprint, the final version is subject to change, of the American Mineralogist (MSA)
Cite as Authors (Year) Title. American Mineralogist, in press.
(DOI will not work until issue is live.) DOI: http://dx.doi.org/10.2138/am-2017-5910

"Revision 1"

Paper #: 5910R

Reconstructive phase transitions induced by temperature in gmelinite-Na zeolite.

ALBERTO ALBERTI,*, GIUSEPPE CRUCIANI, AND ANNALISA MARTUCCI

Department of Physics and Earth Sciences, University of Ferrara, Italy

*E-mail: alb@unife.it; alberto.alberti09@gmail.com

Running title: phase transitions in gmelinite-Na

ABSTRACT

Gmelinite is a natural zeolite whose framework can be described as a parallel stacking of double six rings of tetrahedra in the ABAB sequence. Its space group is $P6_3/mmc$ with a = 13.76 and c = 10.08 Å. This study describes the topological transformations of its Na-form $|Na_{6.98}K_{0.27}Ca_{0.15}(H_2O_{22.43})|[Al_{7.41}Si_{16.55}O_{48}]$-GME which occur when heating in air above 300 °C. '*Ex situ*' X-ray single crystal analysis showed that gmelinite-Na transforms into a new structure with an **AFI**-type topology at about 300 °C. Its space group is $P6/mcc$ with a = 13.80 and c = 8.50 Å.*'In situ'* X-ray powder diffraction patterns highlighted that, in the approximate 330 – 390 °C temperature range, **GME** → **AFI** transformation goes through a new intermediate phase whose topology differs from both **GME** and **AFI**. This phase transforms over the space of a few minutes

into the **AFI**-type phase. This new "transient" phase is characterized by the presence of framework tetrahedra which are only three-connected. Based on real time synchrotron powder diffraction data, the "transient" phase was modelled in space group *P*31*c* with a = 13.97 and c = 9.19 Å. Its crystal structure can be seen as an intermediate step between the **GME** and **AFI** crystal structures. The existence of this intermediate metastable phase could be due to the approximately 2 Å difference in the c parameter between the GME and AFI phases. The c parameter value in the "transient" metastable phase, which is roughly intermediate between the c value in **GME** and **AFI**, suggests that the "transient" phase exists as a way of avoiding the abrupt collapse of the **GME** structure along z direction during the **GME-AFI** topological transformation. The transformation of a natural gmelinite-Na in a material with **AFI** topology shows that it is possible to obtain Al-rich **AFI** materials whose properties are of particular importance in evaluating their potential as catalysts and adsorbents.

Keywords: zeolite, gmelinite-Na, thermal behaviour, phase transitions, **AFI**-type topology

Introduction

Gmelinite is a fairly rare natural zeolite which typically occurs in hydrothermal formations, mainly filling up cavities in basalts. This material is a member of the so-called ABC-6 family. Its framework (IUPAC code **GME**) can be easily described as a parallel stacking of double six rings of tetrahedra (D6R or, according to Smith (2000) hpr polyhedral unit) in the ABAB sequence. UUDD 4-ring chains connect these D6R units. Its framework structure is characterized by a one-dimensional channel parallel to [001] delimited by rings of twelve tetrahedra interconnected via two-dimensional 8-ring channels which are orthogonal to the 12-ring channel, thus forming a three-dimensional channel system. Passaglia et al. (1978) studied the crystal chemistry of gmelinites. The Si/(Si+Al) ratio varies within a fairly restricted range (0.65-0.71). Usually Na is the predominant

extraframework cation, but samples are not infrequently found where Ca is the most abundant cation; in some cases (Malinovskii, 1984; Vezzalini et al., 1990; Luppi et al., 2007) potassium is the most abundant extraframework cation. Consequently, according to the Recommended Nomenclature of the IMA Subcommittee on Zeolites, three separate species must be recognized, gmelinite-Na, -Ca, and –K (Coombs et al., 1997). The crystal structure of gmelinite was determined by Fischer (1966) on a Na-rich sample from Nova Scotia. Structure refinements on gmelinite-Na and gmelinite-Ca were performed by Galli et al. (1982), gmelinite-K by Malinovskii (1984) and Vezzalini et al. (1990), whereas Ba-substituted structure refinement was carried out by Vigdorchik and Malinovskii (1986). In all these samples, two extraframework cation sites were localized, whereas the number of water sites varies according to the most abundant extraframework cation.

The response of zeolitic materials to heating is not only of academic significance but also of potential industrial importance. Thermal effects such as the evolution of H_2O and encapsulated organic species, which modify unit cell volume and pore and channel geometry, affect the adsorption and diffusion of molecules in microporous materials and, consequently, the efficiency of their applications. The structural modifications induced by heating vary remarkably, and often dramatically, as a function of many parameters: topology, framework composition, exchangeable cations, structure directing agents, order-disorder in the framework, location of acid sites, heating modalities and many others. Usually zeolitic materials undergo more or less strong modifications in their structure without topological changes upon heating treatment up to collapse or breakdown (Cruciani, 2006), but materials which undergo topological changes are not infrequent. Alberti and Martucci (2011) observed that reconstructive phase transitions in microporous materials occur as a consequence of T-O-T bridge breaking, in the smallest framework ring, according to a mechanism described by Alberti and Vezzalini (1984) as a ”face sharing tetrahedra” process. There are always water molecules which seem to act as a catalyst in promoting structural modifications.

In an X-ray study on gmelinite-Na dehydration and rehydration processes, Alberti et al. (2010) observed that this mineral transforms into a new phase at about 300 °C whose powder pattern

resembles that of a phase with **AFI** topology. **AFI** topology can be described as columns of six-rings of tetrahedra in the UDUDUD sequence bonded to each other as in tridymite. These columns are connected through UDUD-type 4-rings to delimitate 12-ring channels parallel to [0001] (Wilson et al.,1982; Bennett et al., 1983). The topological symmetry is *P*6/*mcc*, which is also the topochemical symmetry of pure **AFI**-type SSZ-24 siliceous materials (Bialek et al., 1991). The ordered distribution of Al and P in AlPO-5 lowers the topochemical symmetry to the space group *P*6*cc*. Fig. 1 allows us to compare **AFI** topology with **GME** topology. **AFI** topology was firstly found in an aluminophosphate material (AlPO-5), which was synthesized at 150 °C from a hydrothermal system containing an aluminophosphate gel and tetrapropylammonium hydroxide (Wilson et al., 1982). Its crystal structure was resolved by Bennett et al. (1983) by single crystal X-ray diffraction.

The aim of this work is to study the structural features and properties of gmelinite-Na upon heating up to collapse or breakdown. It has been demonstrated that different thermal kinetics, e.g. far-from-equilibrium vs. the near-to-equilibrium conditions (Cruciani, 2006), play a primary role not only in the dehydration mechanism but also in framework bridge breaking. As an example, dehydration causes the breaking of different T-O-T bridges in stellerite (Arletti et al, 2006; Alberti et, 1978) and barrerite (Ori et al. 2009; Alberti and Vezzalini,1978) thus, generating different, new topologies, if heated near to equilibrium conditions (‘*ex situ’*) or far from equilibrium conditions *(‘in situ’*). Therefore, it became evident that studying the thermal behaviour of gmelinite using either *‘ex situ’* or *‘in situ’* techniques would be necessary. As a result, heating processes were performed both in ‘*ex situ*’ or ‘*in situ*’ using X-ray experimental procedures.

Knowledge of gmelinite thermal stability

Kühl and Miale (1978) studied the thermal behaviour of sodium rich gmelinite from Prospect Park, New Jersey, after ion-exchange with NH_4-, K- and Ca. The authors found that NH_4- and K-

forms do not show phase-transformation up to at least 550 °C. On the contrary, Ca-exchanged gmelinite, when heated for 3 hours at 350 °C, transforms into a new, non-identified, phase which is stable at up to 770 °C. Huo (2002) showed that a sodium gmelinite synthesized with a quaternary ammonium template and an Si/Al ratio of about 4, transforms into a new phase with **AFI** topology when calcined for 5 h at 500 °C. An analogous result is obtained when the exchangeable cations are Li, Mg, Ca, and Ba. On the contrary, the K-exchanged gmelinite does not show phase-transformation when calcined up to 700 °C. The transformation of gmelinite-Na, at around 300 °C, into a new phase whose powder pattern resembles that of an AlPO-5 phase was also found by Alberti et al. (2010) in a study on the dehydration and rehydration process of this material. However, strong differences in intensities (see Fig. 2) indicated that the crystal structure of the new phase is significantly different from that of a pure siliceous **AFI**-type material (Bialek et al., 1991).

Experimental

The same gmelinite sample from Flinders, Victoria, Australia, used by Alberti et al. (2010) to follow the '*ex situ'* dehydration-rehydration process in gmelinite-Na was also used in this study. Its chemical composition, which was determined by microprobe and TG analyses is: $|Na_{6.98}K_{0.27}Ca_{0.15}(H_2O_{22.43})|[Al_{7.41}Si_{16.55}O_{48}]$.

a) 'ex situ' X-ray powder diffraction

In order to determine the thermal stability of gmelinite-Na in this study, powders from the sample were heated at steps of 50 °C and a heating rate of 2°C/min. The heated samples were held at the target temperature overnight. At each step, an X-ray powder pattern was collected ('*ex situ')* on a Bruker D8 Advance diffractometer equipped with a Sol-X solid state detector.

b) 'ex situ' X-ray single crystal structure analysis

In order to determine the crystal features of this new phase, several single crystals of gmelinite-Na were heated at 330 °C, heating rate 2°C/min. Most of these crystals fragmented into many small

crystallites, but a few crystals remained sufficiently undamaged to allow single-crystal data collection. The crystal which appeared to be the least damaged was selected and single crystal data collection was performed using a Bruker (Nonius) four-circle Kappa CCD diffractometer equipped with a 2D detector and MoKα radiation. The DENZO-SMN (Otwinowski and Minor 1997) package was used for the refinement of the unit-cell parameters and data reduction. The SHELX-93 (Sheldrik 1993) program was employed for the single crystal structure refinement.

c) 'in situ' synchrotron powder diffraction

'*In situ'* time resolved diffraction measurements were performed at the GILDA-BM8 beamline (now LISA) (ESFR, Grenoble), on powders from the same gmelinite sample from Flinders, Victoria, Australia. The sample was loaded and packed in a 0.3mm diameter Lindemann capillary open at both ends then horizontally mounted on a rotating goniometer head. The capillary was heated '*in situ*' using a hot air stream equipped with a Eurotherm controller; a constant heating rate of 5°C/min was applied, and the sample was heated from 25 °C to 800 °C. The temperature was monitored using a thermocouple inserted at the heating gun opening. The measurements were carried out using the translating image plate (TIP) experimental setup technique. Powder diffraction patterns were continuously recorded during the heating treatment on the 4mm slit-delimited portion of a 2D image plate (Norby, 1977). Monochromatic incident radiation (λ= 0.68881(1) Å) was selected. The distance between the sample and the image plate was 204.7 mm. It was determined by measuring a 0.3 capillary with LaB_6 standard and using the calibration procedure as implemented in the FIT2D program (Hammersley et al., 1994) which was also used to determine the primary beam centre position and the tilting angle of the image plate detector. The temperature resolved diffraction patterns were extracted from the 2D image by integrating them onto 5°C-wide strips with an integration step of 10 °C using locally written routines.

d) IR-NIR spectroscopy and thermal analyses

Infrared (IR) and *Near Infrared* diffuse reflectance (NIR) spectra were recorded using a Bruker IFS88 infrared spectrophotometer. Spectra were recorded in absorbance mode by collecting at least

24 scans with a 6 cm^{-1} resolution. Samples were prepared in KBr pellets. TG and DTG analyses were carried out under a constant flux of air using a Netzsch STA 409 PC LUXX instrument.

Results

a) 'ex situ' X-ray powder diffraction

The *'ex situ'* powder diffraction indicated that no remarkable differences in the patterns exist up to about 280 °C. At 330 °C, the powder pattern showed a phase transition from gmelinite-Na to a new structure whose pattern resembles a structure with an **AFI**-type topology (see Fig. 2). The AFI-type phase is stable up to 830 °C without any relevant loss of crystallinity, and is amorphous at 880 °C.

b)' Ex situ' X-ray single crystal structure analysis

In order to understand the structural features of gmelinite-Na at above 300 °C, X-ray data collection on a single crystal of gmelinite heated to 330 °C was performed according to the procedure described in the experimental section.

From these data, we can reconstruct the precession images of reciprocal planes. Figure 3 shows pictures of the *hk0*, *hk2*, *h0l*, and *hk1*, *hk3* reciprocal planes. A very wide broadening can be observed on the *h0l* plane for *l* odd reflections, whereas this broadening is absent for *l* even reflections. Moreover, a hexagonal image appears in the *hkl* reciprocal planes with *l* odd due to diffuse scattering and some weak, sharp peaks, which obey *p6mm* symmetry, overlapping the diffuse scattering (Fig. 3). These pictures provide useful information on the crystal microstructure, suggesting strong disorder, with significant short range order, at the framework level.

Single crystal structure analysis of this **AFI-type** material was therefore performed, in spite of its unusual set of X-ray data. As a first step, the positional parameters of the SSZ-24 framework (space group *P6/mcc)* as reported by Bialek et al. (1991) in Table 4 provided the starting coordinates. Only *hkl* reflections with *l* even were used. Remarkable modifications in the framework were immediately evident. The occupancy factors of both the tetrahedral cation and the

oxygen atom on the mirror plane orthogonal to the six-fold axis (T1 and O3) were strongly overestimated. Two new maxima at about 1 Å from these atoms, respectively, were evident in the observed and difference Fourier maps. Refinement of coordinates and occupancy factors for these four positions clearly indicated that both T cations and O atoms alternately occupy two different sites with about the same population. In spite of the poor quality of the X-ray diffraction data, and, consequently, of the structure analysis, a framework model was evident. UDUDUD and DUDUDU configurations are present in the 6-rings of tetrahedra with about the same frequency thus alternating randomly. Consequently, this disorder in the (0001) plane reflects in the spread found in *hkl* reflections with *l* odd (see Fig. 3). Figure 4 shows the average structure of the **AFI**-type phase where domains either with UDUDUD or with DUDUDU configurations are present (red and blue tetrahedra, respectively). Refinements in hexagonal space groups with lower symmetry, like *P*6*cc* or *P*6/*m*, indicated the same model. No particular attention was paid to the extraframework content; only a few sites have been taken into account even if other weak maxima appeared in the Fourier syntheses. Owing to poor data quality, a further effort to refine the structure was considered scarcely significant. Thermogravimetric analysis performed four days after heating on the sample heated to 350 °C gave a water loss of about 13% which is by far lower than that found for gmelinite-Na (~20%) (see Fig. S1). Table 1 reports the parameters of the crystal structure analysis. Table 2 reports the atomic coordinates, occupancy and isotropic displacement parameters and Table 3 interatomic distances and angles of the **AFI**-type phase.

In order to understand the process which transforms gmelinite into an AlPO-5-type phase, we can compare **GME** topology with **AFI** topology (see Fig. 1). In **AFI** topology, the gmelinite double 6-rings (Fig. 1a) are substituted by 6-rings of regularly alternated UDUDUD tetrahedra (Fig. 1b). This phase transformation can be described as a “face-sharing tetrahedra” process (Alberti and Vezzalini, 1983). In this process, a T-O-T bridge is broken and one or both tetrahedral cations migrate to generate new tetrahedra where three vertexes remain as previously i.e. common to the previously occupied tetrahedra. The fourth vertex is an oxygen, when it is shared by two tetrahedra,

or an hydroxyl, when it is unshared; it is obvious that only one tetrahedron can be filled once. To date, phase transitions known to cause changes in topology in microporous alumino-silicates and alumino-phosphates are due to this "face-sharing tetrahedra" process (Alberti and Martucci, 2011). By comparing Figure 1a and 1b, it can be observed that in **GME→AFI** transformation the "face-sharing tetrahedra" process occurs in alternated couples of tetrahedra in the 6-rings.

The structural disorder found in this AFI-type phase can be generated by errors in the UDUDUD regular alternation of the tetrahedra as occurs when two adjacent T-O-T bridges break (shown in Fig. 5a) or when disagreeing occurs in T-O-T breaking in the opposite 6-rings of gmelinite framework (Fig. 5b). In both cases, there are defects in the **AFI** structure framework, with some framework tetrahedra being only three connected and, consequently, the presence of T-O-H hydroxyl groups is probable.

To verify whether hydroxyls are present in untreated gmelinite and in its heated phase, a spectroscopic investigation was performed. Figure 6 reports the *infrared* (IR) (Fig. 6a) and the *near infrared* diffuse reflectance spectra (NIR) (Fig. 6b) of untreated and heated gmelinite, respectively. The IR spectra show a very broad band in the 3700-3400 cm^{-1} region, where the ν_{H2O}, ν'_{H2O} and ν_{OH} bands are present, both for untreated and heated gmelinite-Na. Framework hydroxyl combination bands at ~ 4560 cm^{-1} appear in the NIR reflectance spectrum of gmelinite when heated to 350 °C, whereas these bands are absent in the spectrum of untreated gmelinite. These bands are due to the combination of ν_{OH} stretching vibrations with the $\delta_{Si\text{-}O\text{-}H}$ bending vibration, (Cariati et al., 1981 and references therein) by assuming values for these vibration of about 3.600 cm^{-1} and 1.000 cm^{-1}, respectively, according to Langer and Flörke (1974). Therefore, T-O-H groups are present in gmelinite when heated to 350 °C, while they are absent in gmelinite-Na. Thus, confirming the remarkable amount of framework defects in gmelinite-Na after heating. An analogue combination band was found in other zeolites (e.g. Alberti et al., 1983; Alberti et al., 2001) where the aluminosilicate framework is interrupted by the statistical breaking of oxygen bridges, giving rise to partial occupied "face sharing" tetrahedra, as occurs in this case.

As already mentioned in the Experimental section, gmelinite-Na powders when heated '*ex situ*' showed a phase transition to the **AFI**-type phase at 330 °C which is stable up to 830 °C. The powder pattern of the sample when heated to 448 °C (a temperature in the 330-830 °C) was used to ascertain the crystal features of the **AFI**-type phase, and to compare them to what was obtained by single crystal X-ray analysis at 330 °C. Rietveld refinement was performed by starting from the framework coordinates of SSZ-24 which were reported by Bialek et al. (1991) in Table 4. Two new maxima, located near to the T1P and O3P found in the single crystal X-ray analysis (see Table 2) were highlighted in the Fo and ΔF syntheses. Structure refinements, including these new two maxima, converged rapidly providing a model analogue to that obtained using the single crystal, thus confirming the correctness of the framework model. Observed, calculated, and difference profiles of gmelinite-Na, heated to 448 °C are reported in Figure S2. It is noteworthy that *hkl* reflections with *l* were never observed in the experimental pattern

c) 'In situ' synchrotron powder analysis

As reported in the Experimental section, time-resolved synchrotron powder diffraction data on gmelinite-Na were collected at the GILDA (now LISA) beamline at ESRF in Grenoble.

Figure 7 shows the evolution of the X-ray powder diffraction patterns as a function of temperature in the 250-500 °C temperature range during the *'in situ'* experiment. Unit cell parameters in the 25-818 °C temperature range are reported in Table 4, whereas Figure 8 shows their evolution as a function of temperature in the same temperature range. It is evident that the GME→AFI framework transition occurs through three different phases. The first one occurs up to a temperature of about 330° C and corresponds to the GME-type phase. The last phase occurs at about 390° C and exists up to 818° C. Unit cell parameters indicate that this phase corresponds to the AFI-type phase. It is evident that GME-AFI framework transition occurs through another different phase (the second one) in the 330-390 °C temperature range (Figs. 7 and 8, Table 4). It is noteworthy that, according to the results reported in paragraph *a)* of this section, the new phase was

not detected when the powders were heated in the same temperature range (330-390° C). However, the X-ray data were collected many hours after the heating experiment *('ex situ'*), i.e. in near thermodynamic equilibrium conditions. To understand these conflicting results, a second *'in situ'* experiment was carried out in which the heating process was stopped at 343 °C. New powder patterns were collected at this temperature once a minute for a few minutes. The time evolution of these patterns, highlighted that the new phase transforms rapidly into an **AFI**-type phase. This transformation is almost complete after some minutes. The new phase will be called "transient" from now on.

Table 5 reports the unit cell parameters of the three phases obtained by the *'in situ'* powder pattern refinements at 25 °C, 343 °C, and 448 °C, respectively. The *a* cell parameter does not change remarkably, whereas the *c* parameter dramatically shortens and in the "transient" phase is approximately intermediate between the *c* value in gmelinite and in the **AFI**-type phase. The systematic absences in the powder pattern indicate that the space group of the "transient" phase is $P6_3/mmc$ or one of its subgroups ($P6_3mc$, *P*-62*c,* *P*-31*c*, *P*31*c*) but not the *P6mcc* space group, which characterizes AFI topology. No inorganic database reports a phase with these characteristics. In order to solve its crystal structure, the *EXPO2004* program (Altomare et al., 2004) was applied using the *'in situ'* powder pattern collected at 343 °C and the $P6_3/mmc$ space group. The topology of the proposed solution was the same as gmelinite, suggesting that the "transient" phase is probably similar but obviously differs from gmelinite. Trials to solve the structure using the non-isomorphic subgroups $P6_3mc$, *P*-62*c,* *P*-31*c* were unsuccessful. Finally, a trial in the *P*31*c* space group gave promising information. As a result of the different symmetry of $P6_3/mmc$ and *P*31*c* space groups, the only symmetrically independent T site in $P6_3/mmc$ in gmelinite splits into four symmetrically independent T sites in *P*31*c* (T1…T4 in Table 6 and Fig. 9a). One of the models proposed by *EXPO2004* in this space group indicated a new atom at a distance of 1.5 Å from T1 sites and at about 1.5-1.8 Å from three of the four oxygen atoms which coordinate T1. We hypothesized that this site (T1P in Table 6 and Fig. 9a) was a new tetrahedral site related to T1 by a

"face-sharing tetrahedra" process as set out by Alberti and Vezzalini (1983). A Rietveld refinement procedure was then performed in the *P*31*c* space group on the powder pattern collected *'in situ'* at 343 °C. Analysis of Fo and DF syntheses showed a new maximum at about 1.6 Å from T1P (O3P), so that T1P site resulted fourfold coordinated in a tetrahedral configuration (Fig. 9a). Consequently, T1 and T1P tetrahedra become statistically only three-connected. At the same time, parameter *c* shortens by about 0.9 Å with respect to gmelinite (see Table 5). Therefore, the structural analysis performed using the Rietveld method on the *'in situ'* powder pattern collected at 343 °C gave a model of the "transient" phase crystal structure. Figure 9a shows the new structure. This process is the same as is found every time a topological phase transition occurs in a framework structure. It has also been reported in several structures, both aluminosilicates and aluminophosphates, and its characteristics were recently discussed by Alberti and Martucci (2011). Moreover, Rietveld structure refinement showed that T1 and T1P tetrahedra are alternately present in about 50% of cases. A similar level of occupancy was also found for O3 and O3P, thus confirming the correctness of the model. Therefore, in the last refinement cycles, T1, T1P, O3, and O3P occupancy was fixed at 50%. The partial migration of the tetrahedral cation due to a "face-sharing tetrahedra" process has been found in other zeolites (see Alberti and Martucci, 2005, Alberti and Martucci, 2011, and related references). Experimental and refinement parameters of gmelinite-Na, heated to 343°C are reported in Table 7. Observed, calculated, and difference profiles of gmelinite-Na, heated to 343 °C are reported in Figure S2. Table 8 shows the presence of unexpected values in terms of some distances and angles, mainly due to the location of the framework oxygen atom O2'. Some intratetrahedral angles are very narrow (for example O1-T1P-O2' and O1-T1-O2') or wide (O2'-T1-O3 and O2'-T2-O3'). Moreover, the T1-O2'-T2 (109°) intertetrahedral angle and the T1P-O2' (2.01 Å) distance appear unreasonable. When two tetrahedra have a face in common, the T-T distance, (assuming a T-O distance of 1.64 Å as in this case) is about 1.1-1.2 Å. In the "transient" structure, the T1-T1P distance is as wide as 1.69 Å (Table 8). This distance is only possible if at least one of the O2', O1 and O4 oxygen atoms (see Table 6 and Fig. 9a) is shifted a great length

from its initial position when the tetrahedral cation in T1 moves to the T1P position. Table 8 shows that O1 and O4 distances and angles from T1 and T1P are quite regular, so their location does not change dramatically when bonded to T1 or T1P. On the contrary, the O2' oxygen displays very improbable distances and angles, which can only be explained if this anion is located in two different positions depending on whether it is bonded to T1 or T1P. Consequently, this feature can be described as a rotation around the O1-O4 edge of the T1P tetrahedron with respect to the T1 tetrahedron. As a consequence of this rotation, T1, T1P and O3P lie on a straight line (as shown by the T1-T1P-T3P angle of 196°; Table 8) which develops parallel to the *c* direction coming up towards the T3 tetrahedral site. A quite similar situation has recently been found in zeolite levyne (Arletti et al, 2013). Heating causes the breaking of T-O-T bridges and the migration of a framework cation to a new site also in this zeolite, which is related to the first one by the rotation of the new tetrahedron around one edge. This process has been named as 'edge-sharing tetrahedra' by the authors, in analogy with the 'face-sharing tetrahedra' process described before.

When the "transient" phase transforms into the topological **AFI** phase, T1 and O3 sites are emptied as the residual tetrahedral cations in T1 and framework oxygens in O3 migrate to the T1P and O3P sites, respectively. At the same time, T3 cation migrates to a new site (T3P, Fig 9b). For the sake of clarity, a new hypothetical oxygen site representing the equivalent of the O3P oxygen site is also reported in Figure 9b. As a matter of fact, cation T3P now coordinates O3P and forms the new T3P-O3P-T1P oxygen bridge with the consequent generation of an **AFI** topological framework (see Fig. 9c).

Why does the phase transformation gmelinite → **AFI** go through an intermediate "transient" phase? The answer is probably to be found in the approximately 2 Å difference in parameter *c* between the two phases. This large difference prevents the instantaneous formation of new T-O-T bridges as well as an **AFI**-type framework topology. The **GME → AFI** volume decrease is about 15%, which is remarkably less than in other zeolites (e.g. gismondine, natrolite). However, in these

materials the contraction involves all unit cell parameters, whereas in the **GME** → **AFI** transformation, the decrease only involves *c* parameter (see Table 5).

The *c* parameter value in gmelinite-Na (10.08 Å, Alberti et al., 2010) is the sum of the T-T distance (3.14 Å) in the double six ring and the T-T distance (6.94 Å) in the eight ring (see Fig. 1c). According to the *'ex situ'* analysis, the **GME** → **AFI** topological transformation is due to a migration of cations in alternate couples of tetrahedra in the double six ring. If this migration occurs and the *c* parameter does not change dramatically, the distance between the two new tetrahedral sites remains ~4.7 Å, which is too wide for a new T-O-T bridge (~3.0-3.2 Å). In the "transient", this distance reduces to ~3.8 Å, a value which is only about 0.7 Å greater when compared to the ideal distance of 3.0-3.2 Å. This further decrease occurs when the T3 site cation migrates to form the new T-O-T bridge in the **AFI** phase. It is interesting to note that unit cell *a* parameter is more than 0.2 Å larger in the "transient" phase than in gmelinite. This parameter reduces to about the same value as in gmelinite in the **AFI** phase (see Table 5). As a result, the decrease in the unit cell volume is smaller in **GME** → "transient" than in "transient" → **AFI** topological transformations (5.6% and 9.2%, respectively, Table 5).

Implications

The results obtained in the present study confirm that the response of gmelinite-Na to temperature is characterized by peculiar behaviour. When quenched at 100°K, the mineral displays strong disorder in the extraframework content as compared to the location of cations and water molecules at room temperature (Alberti et al., 2010). Moreover, upon heating to over 300 °C, this zeolite transforms into a new phase with **AFI**-type topology. This transformation occurs through a process which is unique in the light of recent knowledge. In fact, at about 300 °C, gmelinite-Na transforms into a phase with new topology where a new tetrahedral site is three-connected. After just a few minutes, this phase transforms into a new one with **AFI**-type topology.

Microporous materials with a structure in which the main feature is a large 12-ring channel, such as gmelinite, zeolite L and mordenite, are important catalysts and adsorbents. One limit to

these materials is their propensity to form intergrowth with other members of the so-called ABC-6 family, resulting in a blocked 12-ring channel and poor sorption properties. In particular, gmelinite frequently forms intergrowths with chabazite (Passaglia et al., 1978). Consequently, its adsorptive properties become essentially those of chabazite. For these reasons, efforts were made to synthesize materials that were free of chabazite intergrowth. The first positive result was obtained by Kerr and co-workers (1977, 1978), who were able to synthesize gmelinite which is free, or substantially free, of chabazite by using quaternary ammonium polymers to force the crystallization of large pore zeolites, in particular gmelinite. Vaughan and Strohmaier (1992) synthesized an aluminosilicate crystalline zeolite, called ECR-26, that has the crystal structure of gmelinite where Al is partially substituted by Cr^{3+}. The presence of Cr^{3+} tends to eliminate the intergrowth of chabazite or related structures. ECR-26 does not require an organic template and has Na as an extraframework cation. After drying at 400° C, this material is able to absorb more than 4% of n-hexane, at room temperature. A silica material with an **AFI** structure such as SSZ-24 (Zones, 1989; Bialek et al., 1991) has been used in catalytic applications and separations, such as the extraction of dimethyl paraffins from isomerates for the production of high octane fuels (Mc Culloch et al. 1992). However, the catalysis, adsorption, and ion-exchange utility of SSZ-24 is limited by the extremely low aluminium content that is made available from the synthesis procedure. The objective of Huo (2002) was to synthesize low silica AFI zeolite catalysts. The findings of Kühl and Miale (1978) led the authors to propose the synthesis of high purity Na-gmelinite, with a Si/Al ratio of around 9, with a quaternary ammonium template. Na-gmelinite calcined in air at 500° C removes the template and transforms Na-gmelinite to Na-AFI zeolite. The new **AFI** material, with an Al content in the framework which is higher than in SSZ-24, will enhance the catalytic utility of SSZ-24. Moreover, it is expected to behave and exhibit similar properties to other low silica zeolites with 12-ring channels. Gmelinite-Na from Flinders, Victoria, Australia is free of chabazite upon X-ray diffraction. Consequently, its properties are of particular importance in evaluating the potential of gmelinite as a catalyst and adsorbent. The present work shows how a natural gmelinite-Na

transforms into a material with **AFI** topology and suggests that it is possible to synthesize gmelinite with very low Si/Al and, consequently, obtain rich Al-**AFI** materials with very interesting potential industrial applications.

Acknowledgments

The authors would like to thank the Centro di Strutturistica Diffrattometrica of the University of Ferrara for the single crystal X-ray data collection. Dr. Marco Scoponi of the Chemistry Department of the University of Ferrara is acknowledged for the Infrared and Near Infrared spectra of gmelinite-Na. The gmelinite specimen used in this study was provided by the Museum of Victoria, Department of Mineralogy and Petrology, Victoria, Australia. The authors wish to thank the Museum for their help. Annalisa Martucci and Giuseppe Cruciani acknowledge MIUR for funding support within the PRIN2008 and PRIN2010 programmes.

References

Alberti, A., and Martucci, A. (2011) Reconstructive phase transitions in microporous materials: rules and factors affecting them. Microporous and Mesoporous Materials, 141, 192-198.

Alberti, A., and Martucci, A. (2005) Phase transformation and structural modifications induced by heating in microporous materials. Studies in Surface Science and Catalysis 155 (A. Gamba, C. Colella and S. Coluccia, Eds.) 19-43.

Alberti, A., and Vezzalini, G . (1978) Crystal structures of heat-collapsed phases of barrerite. Natural zeolites occurrence, properties, use. (L.B. Sand and F. Mumpton Eds.) Pergamon Press, Oxford. 85-98.

Alberti, A., and Vezzalini, G . (1984) Topological changes in dehydrated zeolites: breaking of T-O-T bridges. Proc. Sixth Int. Zeolite Conf., (D. Olson, A. Bisio Eds.) Butterworths, 1984, 834-841.

Alberti, A., Rinaldi,R,. and Vezzalini, G . (1978) Dynamics of dehydration in Stilbite-type structures; stellerite phase B. Physics and Chemistry of Minerals, 2, 365-375.

Alberti, A., Parodi, I., Cruciani, G., Dalconi, M.C., and Martucci, A. (2010) Dehydration and rehydration processes in gmelinite: An in situ X-ray single-crystal study. American Mineralogist, 95, 1773-1782.

Alberti, A., Cariati, F., Erre, L., Piu, P. and Vezzalini, G. (1983) Spectroscopic Investigation on the Presence of OH in Natural Barrerite and in Its Collapsed Phases. Physics and Chemistry of Minerals, 9, 189-191.

Alberti, A., Vezzalini, G., Quartieri, S., Cruciani, G. and Bordiga, S. (2001) Rehydration mechanism in zeolites: reversibilità of T-O-T breaking and of tetrahedral cation migration in brewsterite. Microporous and Mesoporous Materials, 42, 277-287.

Altomare, A., Caliandro, R., Camalli, M., Cuocci, C., Giacovazzo, C., Moliterni, A.G.G., and Rizzi. R. (2004) Automatic structure determination from powder data with *EXPO2004*. J. Applied. Crystallography, 37, 1025-1028.

Arletti, R., Mazzuccato E., and Vezzalini, G. (2006) Influence of dehydration kinetics on T-O-T bridge breaking in zeolites with framework type STI: The case of stellerite. American Mineralogist, 91, 628-634.

Arletti, R., Vezzalini, G., Quartieri, S., Cámara, F., and Alvaro, M. (2013) A new framework topology in the dehydrated form of zeolite levyne. American Mineralogist, 98, 2063-2074.

Baur, W.H. (1992) Self-limiting distortion by antirotating hinges in the principle of flexible but non collapsible frameworks. Journal of Solid State Chemistry, 97, 243-247.

Bennett, J.M., Cohen, J.P., Flanigen, E.M., Pluth, J.J., and Smith J.V. (1983) Crystal Structure of Tetrapropylammonium Hydroxide-Aluminum Phosphate Number 5. ACS Symp. Series, 218, American Chemical Society, Washington, DC, 109-118.

Bialek, R., Meier, W.M., Davis, M., and Annen, M.J. (1991) The synthesis and structure of SSZ-24, the silica analog of AlPO-5. Zeolites, 11, 436-442.

Bish, D.L. (1995) Thermal behavior of Natural Zeolites. Natural Zeolites '93 (D.W. Ming and F.A. Mumpton, Eds.) Int. Commission Natural Zeolites, Brockport, New York.

Cariati, F., Erre, L., Micera, G., Piu, P. and Gessa, C. (1981) Water molecules and hydroxil groups in montmorillonites as studied by near infrared spectroscopy. Clays and Clay Mineralogy. 29, 157-159.

Coombs, D.S., Alberti, A., Armbruster, T., Artioli, G., Coltella, C., Galli, E., Grice, J.D., Liebau, F., Mandarino, J.A., Minato, H., Nickel, E.H., Passaglia, E., Peacor, D.R., Quartieri, S., Rinaldi, R., Ross, M., Sheppard, R.A., Tillmanns, E., and Vezzalini, G. (1997) Recommended nomenclature for zeolite minerals: Report of the Subcommittee on Zeolites of the International Mineralogical Association, Commission on New Minerals and Mineral Names. The Canadian Mineralogist, 35, 1571-1606.

Cronstedt, A.K. (1756) Observation and description of an unknown kind of rock to be named zeolites. Kongl. Vetenskaps Acad. Handl. Stockholm. 17, 120-123 (in Swedish).

Cruciani, G. (2006) Zeolites upon heating: Factors governing their thermal stability and structural changes. Journal of Physics and Chemistry of Solids, 67, 1973-1994.

Daniels, R. H., Kerr, G. I. and Rollmann, L. D. (1978) Cationic Polymers as Templates in Zeolite Crystallization. Journal of the American Chemical Society, 100, 3097-3100.

Fischer, K. (1966) Untersuchung der Kristallstruktur von Gmelinit. Neues Jahrbuch für Mineralogie, Monatshefte, 1966, 1-13.

Galli, E., Passaglia, E., and Zanazzi, P.F. (1982) Gmelinite: structural refinement of sodium-rich and calcium-rich natural crystals. Neues Jahrbuch für Mineralogie, Monatshefte, 1982, 145-155.

Hammersley, A.P., Svensson, S.O., and Thomson, A. (1994) Nuclear Instruments and Methods Phys. Res., Sect. A, 346, 312-321.

Huo, Q. (2002) Synthesis of aluminium rich AFI zeolite. United States Patent 6423295.

Kerr, G. I., and Rollmann L. D. (1977) Direct crystallization of synthetic aluminosilicates. United States Patent 4061717.

Kühl, G.H., and Miale J.N. (1978) Thermal stability of natural gmelinite and some of its ion-exchanged forms. In L.B. Sand and F.A. Mumpton Eds., Natural Zeolites. Occurrence, Properties, Use. p. 421-429. Pergamon Press, Oxford.

Langer, K., and Flörke, O.W. (1974) Near infrared absorption spectra (4.000 – 9.000cm^{-1}) of opals and the role of "water" in these SiO_2xnH_2O minerals. Fortschr. Mineral. 52, 17-51.

Luppi, D., Carbonin, S., Boscardin, M., and Pegoraro, S. (2007) Chabasite e gmelinite del vicentino. Distribuzione e cristallochimica (It.). Rivista Mineralogica Italiana, 31, 8-21.

Malinovskii Yu. A. (1984) The crystal structure of K-gmelinite. Soviet Physics, Crystallography, 29, 256-258.

Mc Culloch, B., Lansbarkis, J. R., Raghuram, S. and Haizmann, R. S. (1992) Extraction of dimethyl paraffins from isomerates. United States Patent 5107052.

Norby, P. (1997) Synchrotron Powder Diffraction using Imaging Plates: Crystal Structure Determination and Rietveld Refinement. Journal of Applied Crystallography, 30, 21-30

Ori, S., Mazzuccato, E., and Vezzalini, G. (2009) Dehydration dynamics of barrerite; An in situ synchrotron XRPD study. American Mineralogist, 94, 64-71.

Otwinowski, Z., and Minor, W. (1997) Processing of X-ray Diffraction Data Collected in Oscillation Mode**.** In C.W. Carter, Jr. and R. M. Sweet. Eds., Methods in Enzymology: Macromolecular Crystallography. Part A, p.307-326. Academic Press, New York.

Passaglia, E., Pongiluppi, D., and Vezzalini, G. (1978) The crystal chemistry of gmelinites. Neues Jahrbuch für Mineralogie, Monatshefte, 1978, 310-324.

Sheldrick, G.M. (1993) SHELXL93, Program for crystal structure determinations. University of Cambridge, Cambridge, UK.

Smith, J.V. (2000) Microporous and other framework materials with zeolite-type structures. In W.H. Baur and R.X. Fischer, Eds., Landolt-Börnstein New Series Group IV, Volume 14, Subvolume A: Tetrahedral frameworks of zeolites, clathrates and related materials. Springer, Berlin.

Vaughan, D. E. W., and Strohmaier, K. G. (1992) Synthesis of ECR-26 (C-2646). United States Patent 5283047.

Vezzalini, G., Quartieri S., and Passaglia E. (1990) Crystal structure of a K-rich natural gmelinite and comparison with the other refined gmelinite samples. Neues Jahrbuch für Mineralogie, Monatshefte, 1990, 504-516.

Vigdorchik A.G., and Malinovskii Yu. A. (1986) Crystal structure of Ba-substituted gmelinite. $Ba_4[Al_8Si_{16}O_{48}]\cdot nH_2O$. Soviet Physics, Crystallography, 31, 519-521.

Wilson, S.T., Lok, B.M., Messina, C.A., Cannan, T.R., and Flanigen, E.M. (1982) Aluminophosphate molecular sieves: a new class of microporous crystalline inorganic solids. Journal of the American Chemical Society, 104, 1146-1147.

Zones, S. (1989) Zeolite SSZ-24. United States Patent 4834958.

This is a preprint, the final version is subject to change, of the American Mineralogist (MSA)
Cite as Authors (Year) Title. American Mineralogist, in press.
(DOI will not work until issue is live.) DOI: http://dx.doi.org/10.2138/am-2017-5910

Figure captions

Figure 1. Comparison between **GME**-type topology (left) and **AFI**-type topology (right) projected along [0001] (a) and [10-10] (b, c) directions.

Figure 2. X-ray powder diffraction pattern of gmelinite-Na heated to 442 °C using an'*ex situ*' experimental procedure (bottom) and an XRPD pattern of synthetic SSZ-24, the pure siliceous analogue of AlPO4-5, (top) calculated from the parameters in Table 4, Bialek et al. (1991).

Figure 3. Reconstructions of precession images from collected frames showing reciprocal planes of gmelinite-Na heated to 330 °C using *'ex situ'* X-ray single crystal experimental procedure

Figure 4. Disordered crystal structure of the **AFI**-type phase as obtained by gmelinite-Na heated to 330 °C ('*ex situ*' X-ray single crystal analysis). Red and blue tetrahedra represent domains with UDUDUD or with DUDUDU configurations of tetrahedra, respectively (see text)

Figure 5. Possible causes of structural disorder in the A**FI**-type phase. Breaking of two adjacent T-O-T bridges in a 6-ring of gmelinite framework (a). Disagreeing occurs in T-O-T breaking in opposite 6-rings of gmelinite framework (b) (see text)

Figure 6. *Infrared* (IR) (a) and *Near Infrared* diffuse reflectance (NIR) (b) spectra of gmelinite-Na at room temperature (red) and heated to 350 °C (blue).

Figure 7. Thermo-diffractogram of gmelinite-Na in the T range 250-500°C as recorded on the imaging plate of the *'in situ'* powder experiment. The 2-theta scale is approximate. Dashed vertical lines mark the boundaries of the "transient" phase.

Figure 8. Temperature dependence of the unit-cell parameters of gmelinite-Na during the '*in situ*' experiment. Data are normalized with respect to those for gmelinite-Na at 25 °: Error bars are smaller than symbols

Figure 9. Evolution of the crystal structure of gmelinite-Na in the course of gmelinite-Na → "transient" → **AFI** reconstructive transformations. The transformation process gmelinite → "transient" phase is shown in Figure 9a, the transformation process "transient" → **AFI**-type phase is shown in Figures 9b and 9c (see text)

This is a preprint, the final version is subject to change, of the American Mineralogist (MSA)
Cite as Authors (Year) Title. American Mineralogist, in press.
(DOI will not work until issue is live.) DOI: http://dx.doi.org/10.2138/am-2017-5910

Figure 1

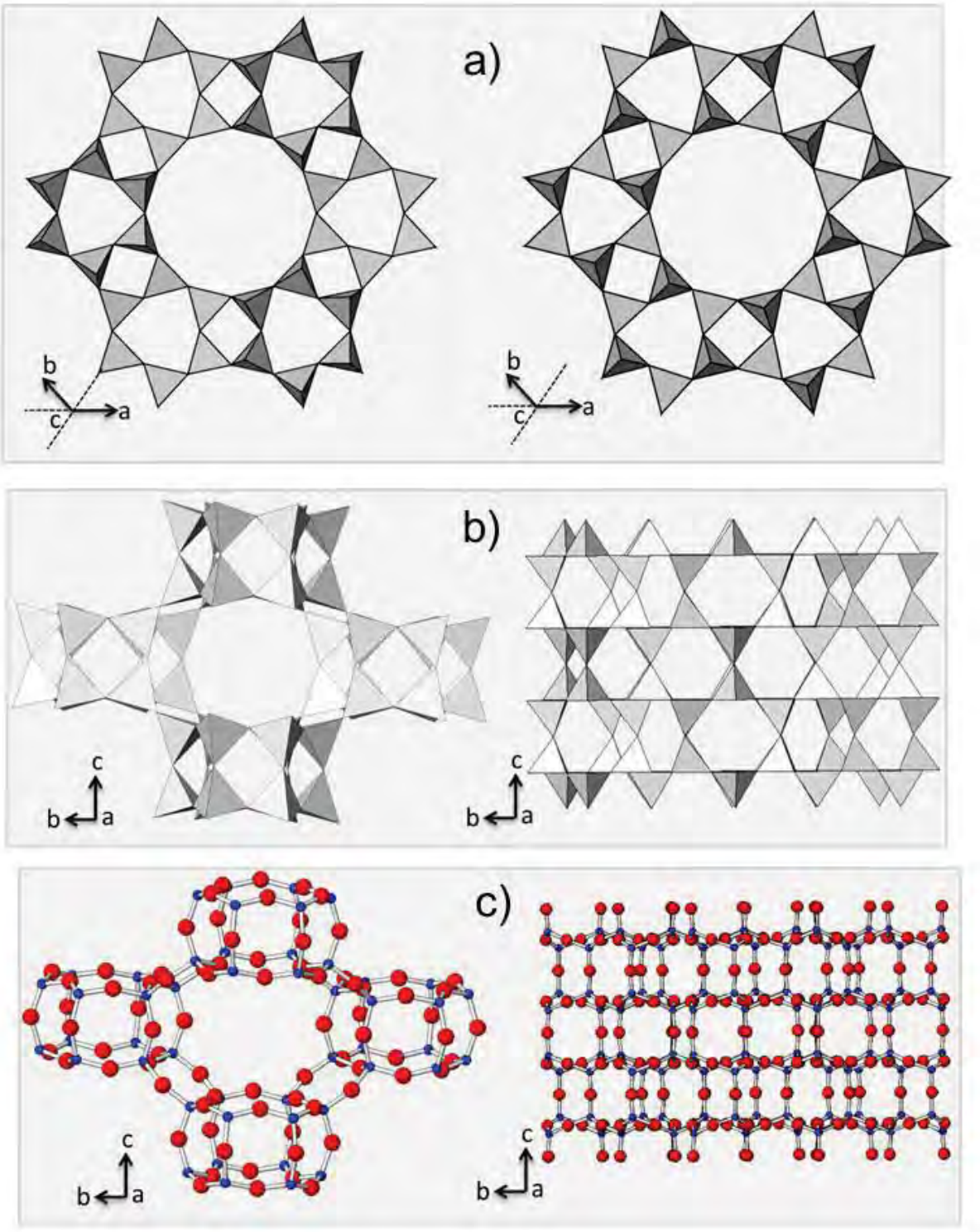

This is a preprint, the final version is subject to change, of the American Mineralogist (MSA)
Cite as Authors (Year) Title. American Mineralogist, in press.
(DOI will not work until issue is live.) DOI: http://dx.doi.org/10.2138/am-2017-5910

Figure 2

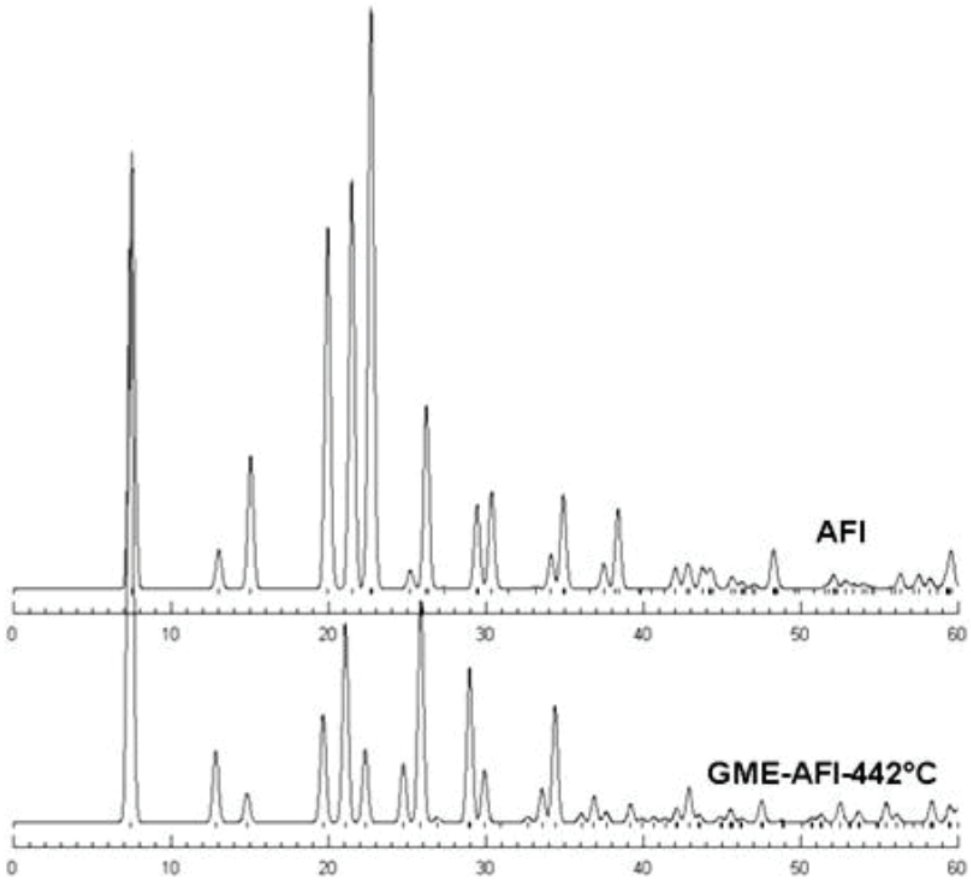

This is a preprint, the final version is subject to change, of the American Mineralogist (MSA)
Cite as Authors (Year) Title. American Mineralogist, in press.
(DOI will not work until issue is live.) DOI: http://dx.doi.org/10.2138/am-2017-5910

Figure 3

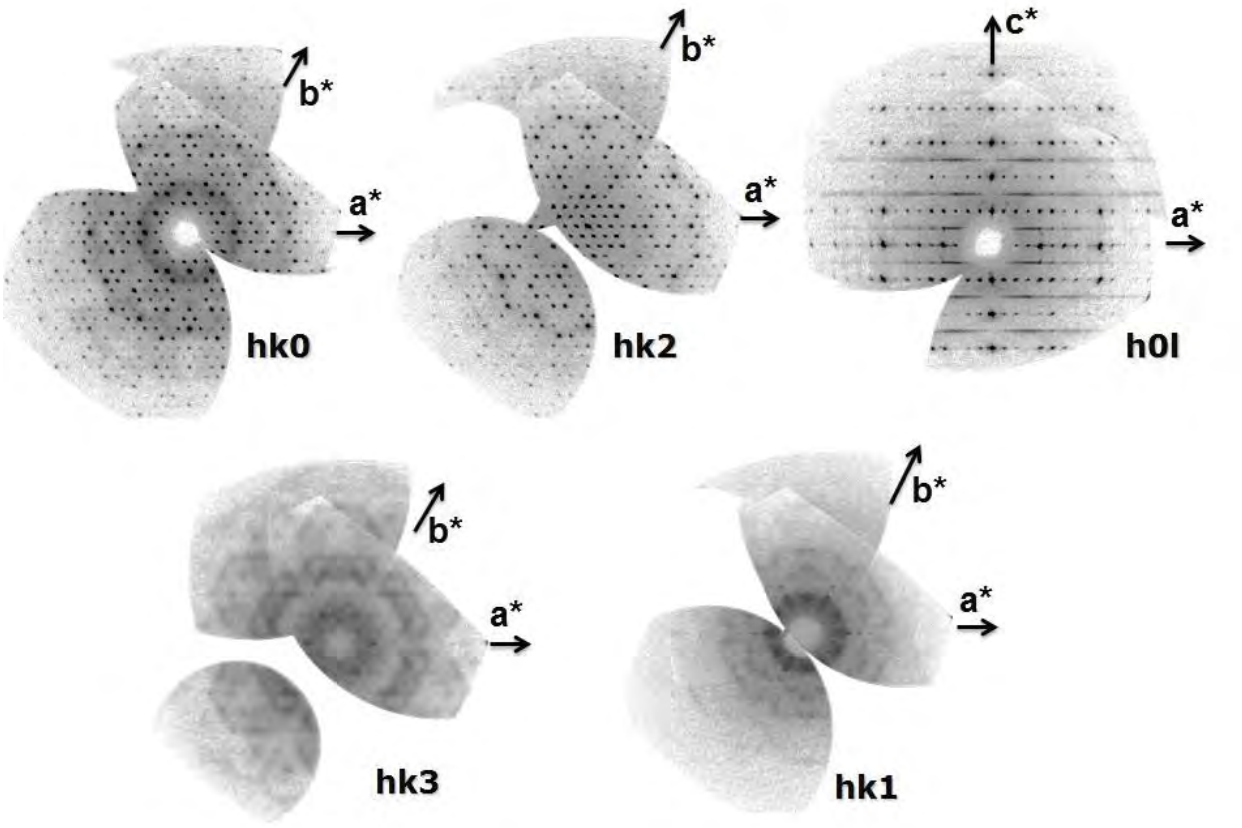

This is a preprint, the final version is subject to change, of the American Mineralogist (MSA)
Cite as Authors (Year) Title. American Mineralogist, in press.
(DOI will not work until issue is live.) DOI: http://dx.doi.org/10.2138/am-2017-5910

Figure 4

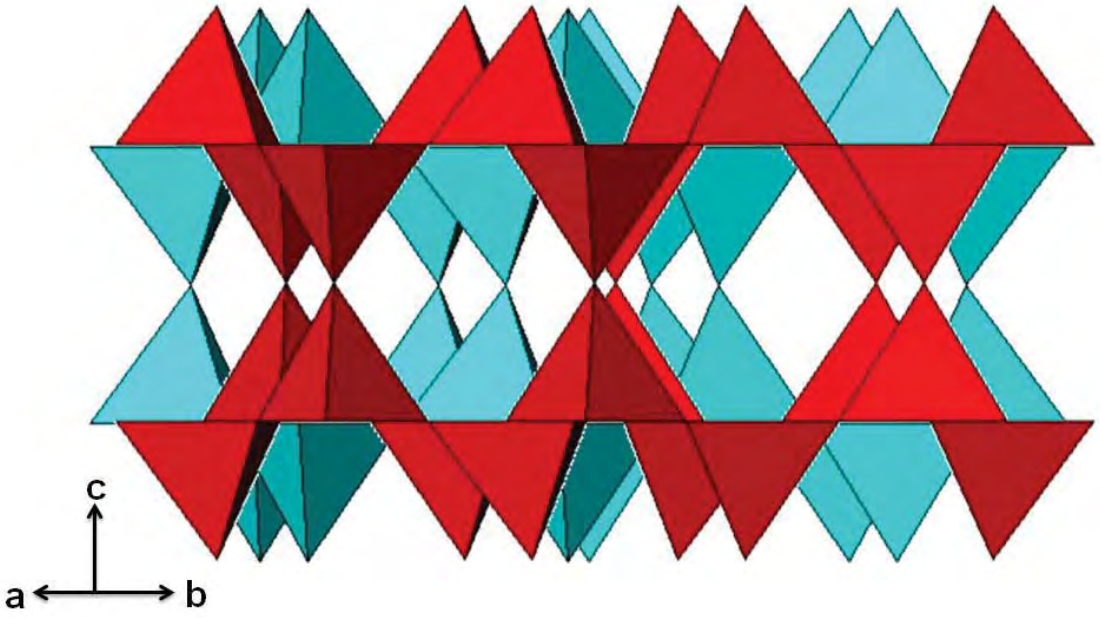

This is a preprint, the final version is subject to change, of the American Mineralogist (MSA)
Cite as Authors (Year) Title. American Mineralogist, in press.
(DOI will not work until issue is live.) DOI: http://dx.doi.org/10.2138/am-2017-5910

Figure 5

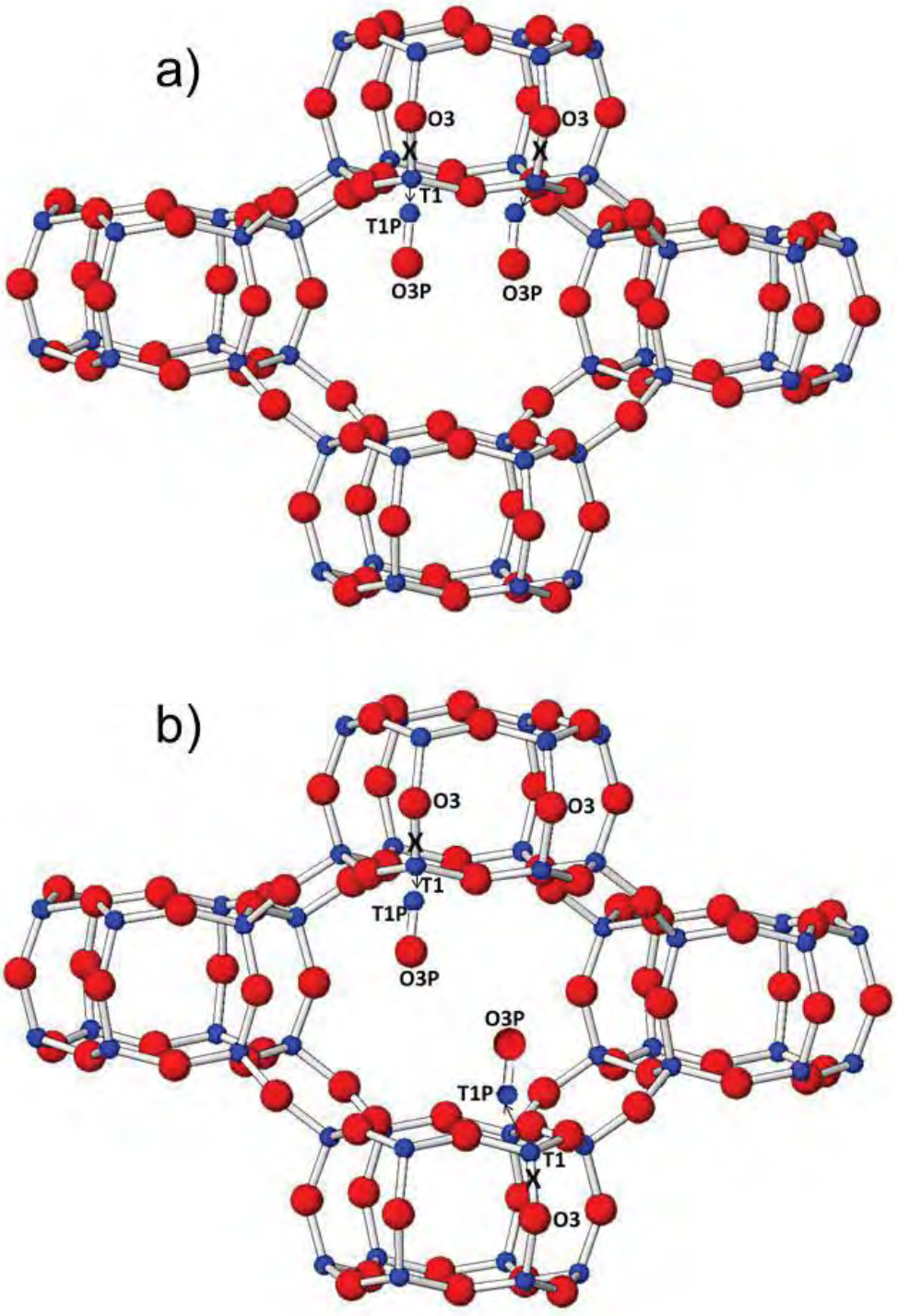

This is a preprint, the final version is subject to change, of the American Mineralogist (MSA)
Cite as Authors (Year) Title. American Mineralogist, in press.
(DOI will not work until issue is live.) DOI: http://dx.doi.org/10.2138/am-2017-5910

Figure 6

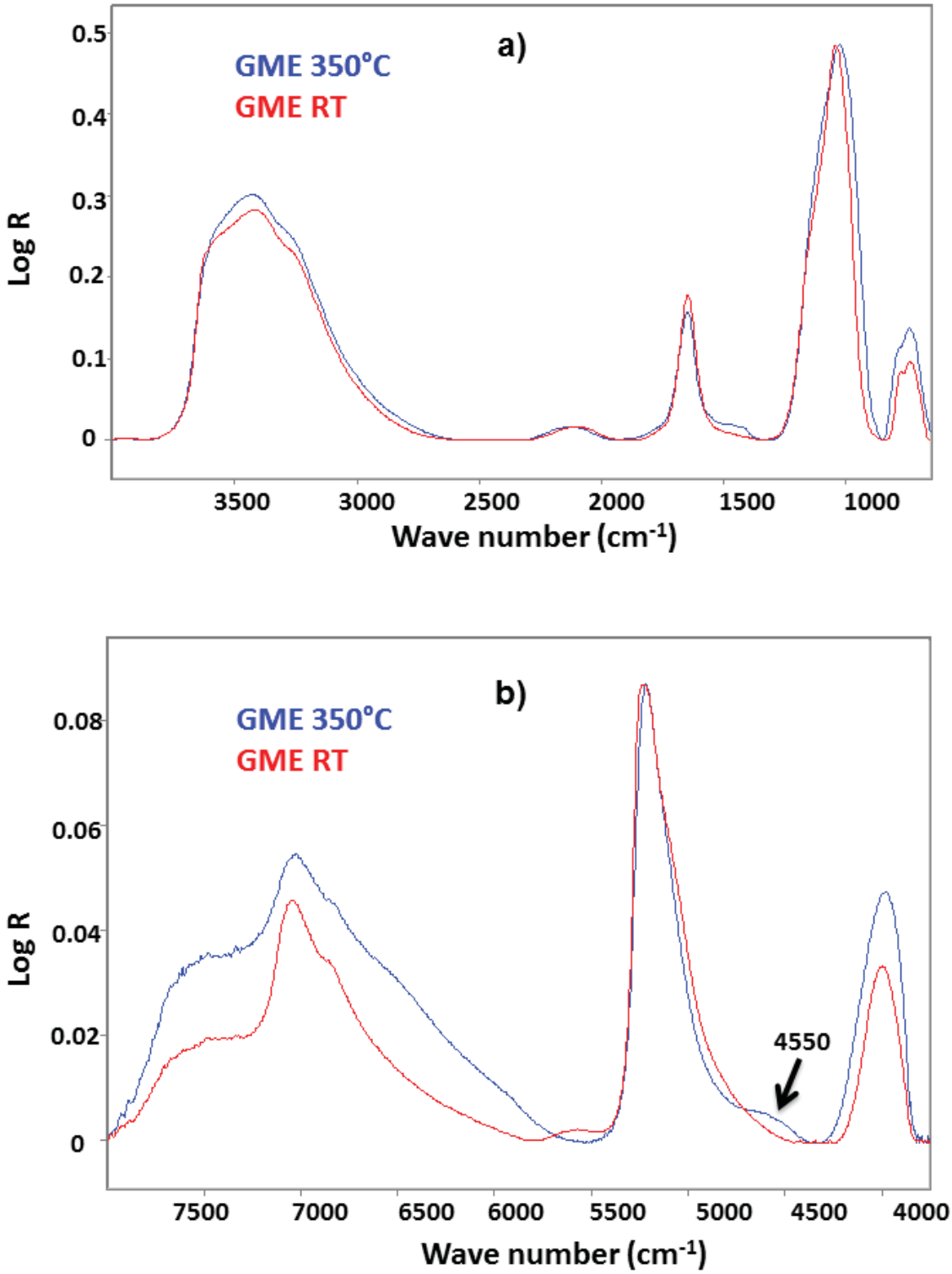

This is a preprint, the final version is subject to change, of the American Mineralogist (MSA)
Cite as Authors (Year) Title. American Mineralogist, in press.
(DOI will not work until issue is live.) DOI: http://dx.doi.org/10.2138/am-2017-5910

Figure 7

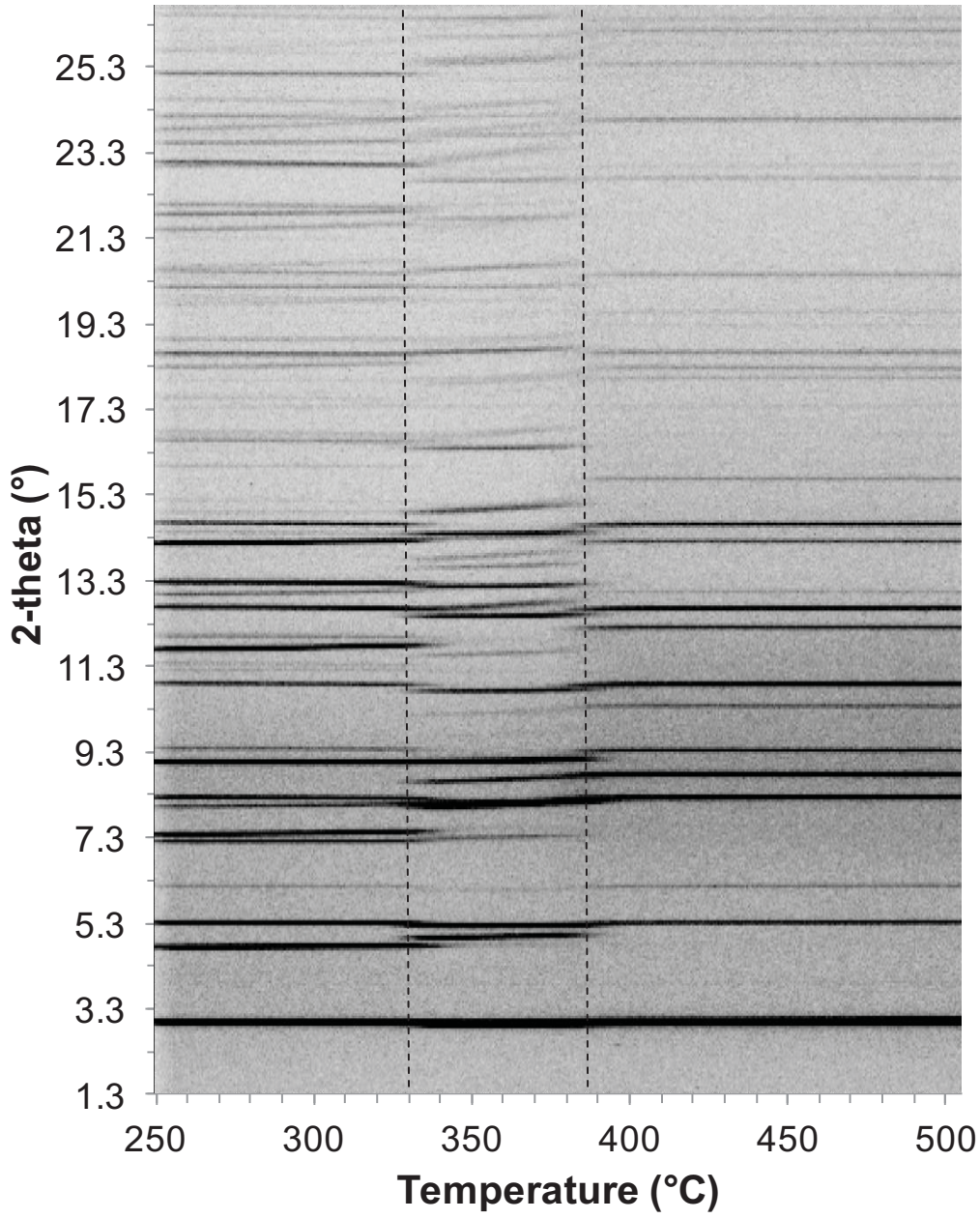

This is a preprint, the final version is subject to change, of the American Mineralogist (MSA)
Cite as Authors (Year) Title. American Mineralogist, in press.
(DOI will not work until issue is live.) DOI: http://dx.doi.org/10.2138/am-2017-5910

Figure 8

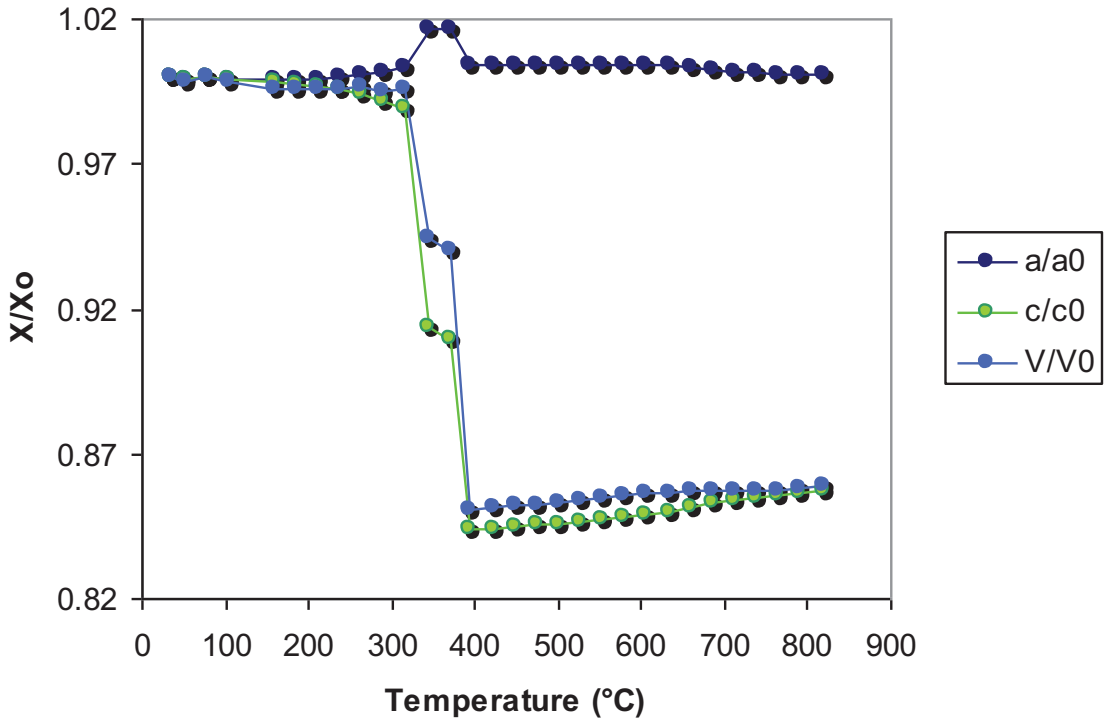

This is a preprint, the final version is subject to change, of the American Mineralogist (MSA)
Cite as Authors (Year) Title. American Mineralogist, in press.
(DOI will not work until issue is live.) DOI: http://dx.doi.org/10.2138/am-2017-5910

Figure 9

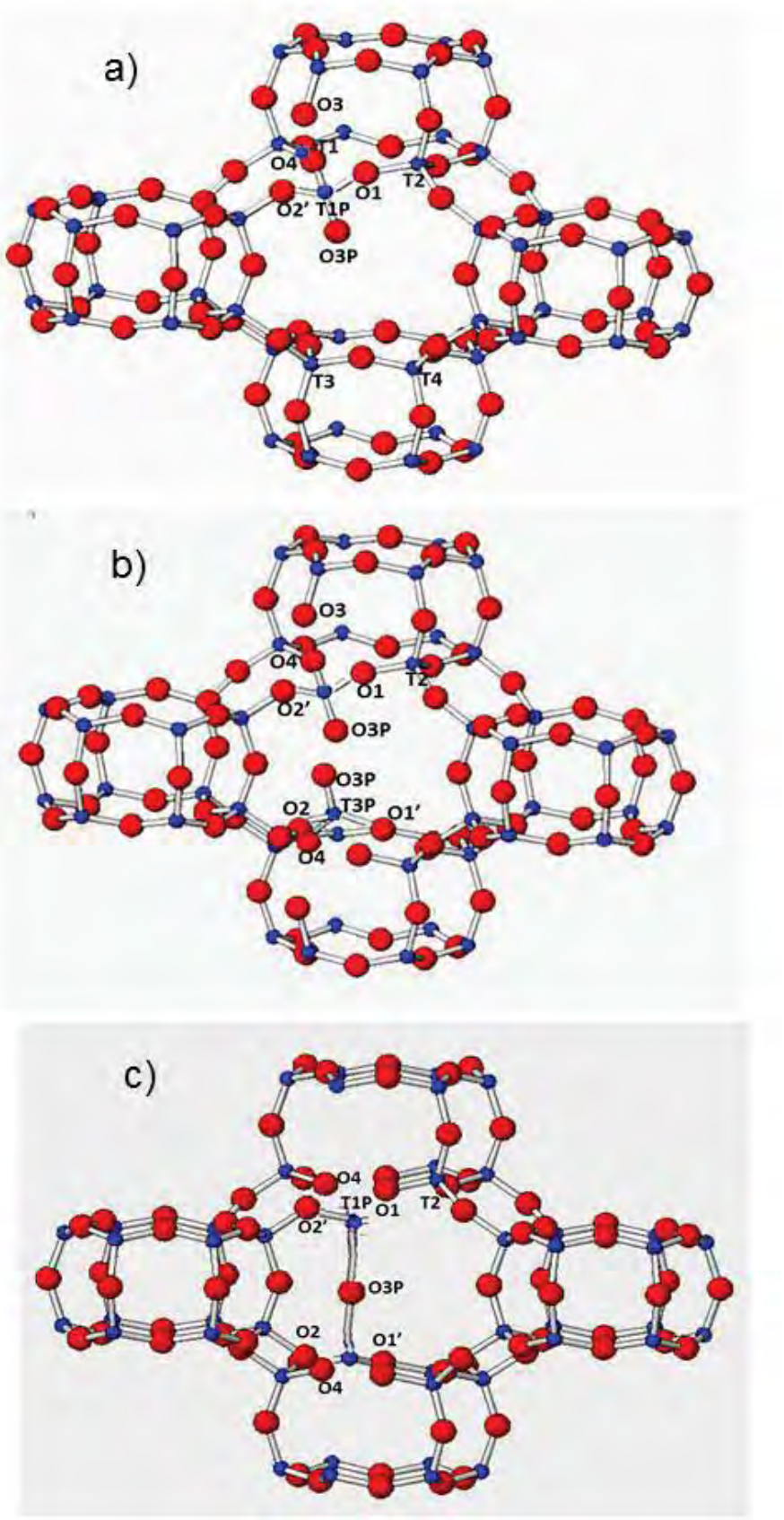

This is a preprint, the final version is subject to change, of the American Mineralogist (MSA)
Cite as Authors (Year) Title. American Mineralogist, in press.
(DOI will not work until issue is live.) DOI: http://dx.doi.org/10.2138/am-2017-5910

Table 1. *'Ex situ'* single crystal structure refinement parameters of gmelinite-Na heated to 330° C, data collected at 25° C (**AFI**-type phase)..

Temperature	**330° C**
a (Å)	13.843(1)
c (Å)	8.433(1)
V(Å^3)	1399.5(2)
Space group	*P6/mcc*
Maximum 2θ	60.0°
Measured reflections	4035
Unique reflections	444
Reflection with Fo>4σ(Fo)	375
R_{int}(%)	6.1
$R1_{all}$(%)	22.2
$wR2_{all}$(%)	54.9
$R1_{obs}$(%)	21.0
$wR2_{obs}$(%)	52.9
$GooF_{all}$	1.02
$GooF_{obs}$	1.02
No. of parameters	36
$\Delta\rho_{max}$ and $\Delta\rho_{min}$ (e/Å^3)	2.6/-1.4

This is a preprint, the final version is subject to change, of the American Mineralogist (MSA)
Cite as Authors (Year) Title. American Mineralogist, in press.
(DOI will not work until issue is live.) DOI: http://dx.doi.org/10.2138/am-2017-5910

Table 2. Atomic coordinates, occupancy and isotropic displacement parameter of gmelinite-Na heated to 330 °C, data collected at 25° C, using '*ex situ*' single crystal (**AFI**-type phase).

Atom	x	y	z	Occ.	Uiso
T1	0.4706(8)	0.3406(7)	0.1847(10)	0.5	0.027(3)
T1P	0.4449(8)	0.3306(6)	0.3152(9)	0.5	0.024(2)
O1	0.2096(5)	0.4192(10)	0.25	1.0	0.050(3)
O2	0.3705(13)	0.0	0.25	1.0	0.088(5)
O3	0.510(3)	0.352(3)	0.0	0.5	0.061(9)
O4	0.5805(9)	0.4196(9)	0.25	1.0	0.102(6)
O3P	0.412(4)	0.321(3)	0.5	0.5	0.062(9)
Na	0.6667	0.3333	0.0	0.38(4)	0.14(1)
W1	0.039(11)	0.219(10)	0.328(17)	0.48(1)	0.26(9)
W2	0.220(7)	0.192(6)	0.0	0.32(6)	0.10(3)
W3	0.294(6)	0.215(4)	0.0	0.55(7)	0.09(1)

Table 3. Interatomic distances (Å) in gmelinite-Na heated to 330°C, data collected at 25° C, using '*ex situ*' single crystal procedure (**AFI-**type phase).

T1-O1	1.68(1)	T1P-O1	1.63(1)
T1-O2	1.72(1)	T1P-O2	1.50(1)
T1-O3	1.63(1)	T1P-O3P	1.61(2)
T1-O4	1.47(2)	T1P-O4	1.74(1)
O1-T1-O2	101(1)	O1-T1P-O2	115(1)
O1-T1-O3	111(1)	O1-T1P-O4	103(1)
O1-T1-O4	114(1)	O1-T1P-O3P	110(1)
O2-T1-O3	124(1)	O2-T1P-O4	109(1)
O2-T1-O4	111(1)	O2-T1P-O3P	100(1)
O3-T1-O4	96(1)	O4-T1P-O3P	122(2)
T1-T1P	1.14(1)		
T1-O1-T1	137(1)	T1-O2-T1	147(1)
T1-O3-T1	145(3)	T1-O4-T1	151(2)
T1P-O1-T1P	158(1)	T1P-O2-T1P	162(2)
T1P-O3P-T1P	151(3)	T1P-O4-T1P	143(1)
Na-O4 [x3]	2.30(4)	Na-O3 [x6]	2.95(2)
W1-W1	1.62(28)	W1-W2	1.66(15)
W1-W3	2.17(15)	W1-W1	2.34(26)
W1-O2	2.51(12)	W1-W3	2.57(14)
W1-W2	2.55(14)	W1-O1	2.68(13)
W1-O3P	2.80(13)	W1-W2	2.77(15)
W1-W3	2.91(14)	W1-W1	2.79(12)
W2-W3	0.90(8)	W2-W1 [x2]	1.66(15)
W2-W1 [x2]	2.55(14)	W2-O3P	2.64(8)
W2-W1 [x2]	2.77(15)	W2-W2 [x2]	2.88(8)
W2-W3	2.94(11)	W3-W1 [x2]	2.17(15)
W3-O3P	2.55(6)	W3-W1 [x2]	2.57(14)
W3-O3	2.63(8)	W3-O1 [x2]	2.76(5)
W3-O2 [x2]	2.81(4)	W3-O3P	2.91(8)

Note: Estimated standard deviations in parentheses refer to the last digit.

Table 4. Unit cell parameters of gmelinite-Na versus temperature by XRPD '*in situ*' procedure

T (°C)	a	c	Vol	a/a_0	c/c_0	V/V_0
25	13.744(1)	10.055(1)	1644.7(1)	1.000	1.000	1.000
52	13.737(1)	10.050(1)	1642.5(1)	1.000	1.000	0.999
79	13.744(1)	10.055(1)	1644.7(1)	1.000	1.000	1.000
105	13.738(1)	10.049(1)	1642.6(1)	1.000	0.999	0.999
158	13.729(1)	10.037(1)	1638.5(1)	0.999	0.998	0.996
184	13.730(1)	10.031(1)	1637.7(1)	0.999	0.998	0.996
211	13.734(1)	10.026(1)	1637.7(1)	0.999	0.997	0.996
237	13.744(1)	10.012(1)	1637.9(1)	1.000	0.996	0.996
263	13.756(1)	10.000(1)	1638.7(1)	1.001	0.995	0.996
290	13.767(1)	9.969(1)	1636.1(1)	1.002	0.991	0.995
316	13.789(1)	9.948(1)	1638.2(1)	1.003	0.989	0.996
343	13.969(7)	9.191(10)	1553.0(16)	1.016	0.914	0.944
369	13.970(7)	9.148(10)	1546.0(16)	1.016	0.910	0.940
395	13.799(1)	8.485(1)	1399.2(1)	1.004	0.844	0.851
422	13.800(1)	8.490(1)	1400.1(1)	1.004	0.844	0.851
448	13.802(1)	8.495(1)	1401.4(1)	1.004	0.845	0.852
475	13.802(1)	8.499(1)	1402.2(1)	1.004	0.845	0.853
501	13.804(1)	8.505(1)	1403.6(1)	1.004	0.846	0.853
527	13.805(1)	8.510(1)	1404.6(1)	1.004	0.846	0.854
554	13.804(1)	8.521(1)	1406.2(1)	1.004	0.847	0.855
580	13.802(1)	8.530(1)	1407.3(1)	1.004	0.848	0.856
606	13.801(1)	8.538(1)	1408.5(1)	1.004	0.849	0.856
633	13.799(1)	8.547(1)	1409.3(1)	1.004	0.850	0.857
659	13.792(1)	8.559(1)	1410.0(1)	1.004	0.851	0.857
686	13.782(1)	8.575(1)	1410.5(1)	1.003	0.853	0.858
712	13.769(1)	8.586(1)	1409.8(1)	1.002	0.854	0.857
738	13.762(1)	8.596(1)	1410.0(1)	1.001	0.855	0.857
765	13.759(1)	8.605(1)	1410.7(1)	1.001	0.856	0.858
791	13.758(1)	8.612(1)	1411.8(1)	1.001	0.857	0.858
818	13.759(1)	8.618(1)	1412.8(1)	1.001	0.857	0.859

This is a preprint, the final version is subject to change, of the American Mineralogist (MSA)
Cite as Authors (Year) Title. American Mineralogist, in press.
(DOI will not work until issue is live.) DOI: http://dx.doi.org/10.2138/am-2017-5910

Table 5 Unit cell parameters and Space Groups

	a(Å)	*c*(Å)	V(Å^3)	Space Group
Gmelinite 25°C "in situ" data	**13.744(1)**	**10.055(1)**	**1644.7(1)**	***P* 63/m m c**
"transient"phase 343°C "in situ" data	**13.969(7)**	**9.191(10)**	**1553.0(16)**	***P* 31c**
AFI-type phase 448°C "in situ" data	**13.802(1)**	**8.495(1)**	**1401.4(1)**	***P* 6/m c c**

Δc 35°C – transient 8.6% Δc transient – AFI 7.6% Δc 35°C – AFI 15.5%
ΔV 35°C – transient 5.6% ΔV transient – AFI 9.7% ΔV 35°C – AFI 14.8%

This is a preprint, the final version is subject to change, of the American Mineralogist (MSA)
Cite as Authors (Year) Title. American Mineralogist, in press.
(DOI will not work until issue is live.) DOI: http://dx.doi.org/10.2138/am-2017-5910

Table 6. Experimental and refinement parameters of gmelinite-Na heated to 343 °C ("transient" phase) by XRPD '*in situ*" procedure.

Gmelinite-Na 343 °C	
Space group	*P31c*
***a*(Å)**	13.972(7)
***c*(Å)**	9.188 (10)
***V*(Å^3)**	1553.4(19)
R_{wp}	16.75
R_p	13.81
R_F^2	18.45
N° Reflections	2861
Nobs	775
N° Variables	106

TABLE 7. Atomic coordinates, occupancy and temperature factor of gmelinite-Na heated to 343 °C ("transient" phase) by XRPD 'in situ' procedure.

Atoms	x	y	z	Occ.	Uiso
T1	0.451(1)	0.117(1)	0.109	0.5	0.052(5)
T2	0.479(1)	0.352(1)	0.081(1)	1.0	0.042(3)
T3	0.444(1)	0.113(1)	0.442(1)	1.0	0.042(3)
T4	0.447(1)	0.338(1)	0.421(5)	1.0	0.042(3)
T1P	0.416(1)	0.126(1)	-0.064(1)	0.5	0.052(5)
O1	0.444(1)	0.223(1)	0.057(1)	1.0	0.063(6)
O1'	0.435(2)	0.222(1)	0.486(1)	1.0	0.063(6)
O2	0.139(1)	0.569(1)	-0.018(1)	1.0	0.063(6)
O2'	0.600(1)	0.432(1)	0.011(1)	1.0	0.063(6)
O3	0.419(1)	0.067(1)	0.275(1)	0.5	0.063(6)
O3'	0.430(2)	0.326(1)	0.250(1)	1.0	0.063(6)
O4	0.364(1)	-0.007(1)	0.517(1)	1.0	0.063(6)
O4'	0.376(1)	0.379(1)	0.521(2)	1.0	0.063(6)
O3P	0.374(2)	0.129(1)	-0.230(1)	0.5	0.063(6)
Na1	0.333	0.667	0.145(11)	1.0	0.091(11)
Na2	0.667	0.333	0.070(10)	0.241(7)	0.071(3)
W1	0.239(5)	0.166(6)	0.431(5)	0.445(9)	0.039(3)

Table 8. Interatomic distances (Å) and angles (°) in the framework in gmelinite-Na heated to 343°C ("transient" phase) by XRPD 'in situ' procedure

T1-O1	1.61(1)	T2-O1	1.63(1)
T1-O2'	1.68(1)	T2-O2'	1.63(1)
T1-O3	1.64(1)	T2-O3'	1.66(1)
T1-O4	1.62(1)	T2-O4'	1.68(1)
T3-O1'	1.63(1)	T4-O1'	1.63(1)
T3-O2	1.64(1)	T4-O2	1.63(1)
T3-O3	1.64(1)	T4-O3'	1.64(1)
T3-O4	1.63(1)	T4-O4'	1.64(1)
T1P-O1	1.64(1)	T1-T1P	1.69(1)
T1P-O2'	2.01(1)		
T1P-O4	1.64(1)		
T1P-O3P	1.64(1)		
O1-T1-O2'	87(1)	O1-T2-O2'	110(1)
O1-T1-O3	122(1)	O1-T2-O3'	91(1)
O1-T1-O4	113(1)	O1-T2-O4'	111(1)
O2'-T1-O3	133(1)	O2'-T2-O3'	134(1)
O2'-T1-O4	101(1)	O2'-T2-O4'	114(1)
O3-T1-O4	100(1)	O3'-T2-O4'	94(1)
O1'-T3-O2	108(1)	O1'-T4-O2	104(1)
O1'-T3-O3	120(1)	O1'-T4-O3'	107(1)
O1'-T3-O4	121(1)	O1'-T4-O4'	113(1)
O2-T3-O3	107(1)	O2-T4-O3'	116(1)
O2-T3-O4	104(1)	O2-T4-O4'	97(1)
O3-T3-O4	95(1)	O3'-T4-O4'	119(1)
O1-T1P-O2'	75(1)	T1-O1-T2	149(1)
O1-T1P-O4	110(1)	T3-O1'-T4	140(1)
O1-T1P-O3P	124(1)	T1-O2'-T2	109(1)
O2'-T1P-O4	88(1)	T1-O3-T3	139(1)
O2'-T1P-O3P	130(1)	T1-O4-T3	156(1)
O4-T1P-O3P	119(1)	T2-O4'-T4	152(1)
T2-O1-T1P	145(1)	T2-O3'-T4	152(1)
T3-O2-T4	141(1)	T3-O4-T1P	128(1)
T2-O2'-T1P	147(1)	T1-T1P-O3P	176(1)

Note: Estimated standard deviations in parentheses refer to the last digit.